Relation Between Anharmonicity of Free Energy Profile and Spectroscopy in Solvation Dynamics: Differences in Spectral Broadening and Peak Shift in Transient Hole-Burning Spectroscopy Studied by Equilibrium Molecular Dynamics Simulation

Tsuyoshi Yamaguchi,[1,*] *Norio Yoshida*,[2] *and Katsura Nishiyama*[3,*]

[1]Graduate School of Engineering, Nagoya University, Chikusa, Nagoya, 464–8603, Japan

[2]Department of Chemistry, Graduate School of Science, Kyushu University, Nishi-ku, Fukuoka 819–0395, Japan

[3]Department of Environmental Science and Technology, Meijo University, Tempaku, Nagoya 468–8502, Japan

ABSTRACT

Solvation dynamics is used to monitor the time-dependent fluctuation of solvent, which plays an essential role in chemical reactions in solution. Transient hole-burning spectroscopy, in which a ground-state depletion (hole) formed by a laser pulse is observed, can be used to monitor solvation dynamics. Previous experiments demonstrated that the hole bandwidth relaxes an order of magnitude slower than the hole peak shift in organic solute–solvent systems. However, the detailed mechanisms behind this are still unclear. In this study, we developed a methodology to calculate transient hole spectra using *equilibrium* molecular dynamics simulation, in which a series of time-dependent system ensembles is accumulated to derive the appropriate dynamic properties. The simulated transient hole spectra adequately reproduced previous spectroscopic results. The different hole bandwidth and peak shift dynamics are ascribed to a non-Gaussian property, or anharmonicity of the free energy profile with respect to the solvation coordinate.

1. Introduction

When modeling a chemical reaction in solution, we often assume an adiabatic and harmonic potential along a reaction coordinate. A reactant, which is typically expressed with a Gaussian distribution, stays in the bottom of the potential. The reactant then transfers to the product potential, with a help of solvent fluctuation. Therefore, solvent fluctuation is indeed essential to understand general chemical reactions in solution.

An approach to detect solvent fluctuation is solvation dynamics, where an ultrafast laser pulse is used to monitor solvent reorganization in response to an abrupt change of the solute electronic-structure. Various methods, such as time-resolved fluorescence,[1-3] photon echo,[4] or transient hole-burning spectroscopy,[5-10] have been applied to solvation dynamics. Recent efforts on solvation dynamics measure proteins[11] and dynamics under a confinement[12], or involve femtosecond X-ray emission spectroscopy.[13]

A vast majority of experiments on solvation dynamics use time-resolved fluorescence spectroscopy, due to its simplicity of experimental procedures and data analysis. However, time-resolved fluorescence spectroscopy inherently includes solute excited-state, whereas transient hole-burning spectroscopy monitors ground-state dynamics. This aspect may serve as an advantage to choose transient hole-burning spectroscopy; if thermal excitation concerning the ground-state dynamics is more important, for example. From a viewpoint of application, a transient[14] or permanent[15] spectral hole can be also used for drawing energy landscapes of proteins or for optical quantum memory, respectively.

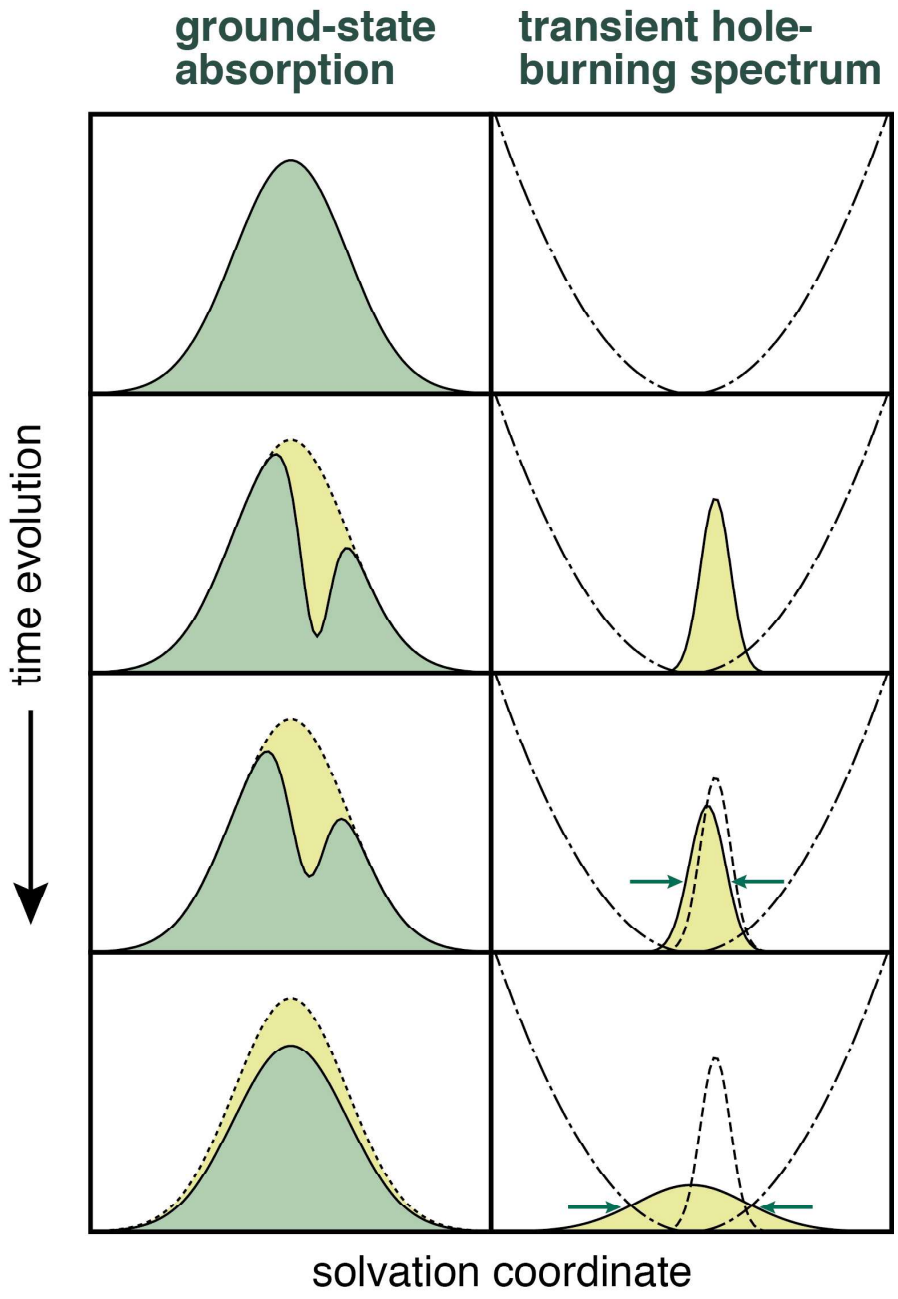

Chart 1. Schematic diagram of transient hole-burning spectroscopy. A laser pulse removes a part of the ground-state distribution (the left column). The depletion in the ground state, or the transient hole-burning spectrum, undergoes relaxation driven by solvent fluctuation (right). After the relaxation is complete, the transient hole-burning spectrum agrees with the absorption spectrum.

Chart 1 shows a schematic of transient hole-burning spectroscopy to detect solvation dynamics. An excitation laser pulse removes the ground-state distribution, which corresponds to the transient hole-burning. The hole-burning spectrum experiences dynamic relaxation in its spectral peak and bandwidth, which is driven by solvent fluctuation. After the relaxation is accomplished, its spectral peak and bandwidth agree with the ground-state absorption spectrum.

In transient hole-burning spectroscopy, as in time-resolved fluorescence spectroscopy, we observe the time evolution of the spectral peak $\tilde{\nu}(t)$ and bandwidth $\tilde{\sigma}^2(t)$, at time t after the excitation. Dynamic response functions derived from these physical quantities, $S_\nu(t)$ and $S_\sigma(t)$, respectively, are introduced:[1, 16]

$$S_\nu(t) = \frac{\tilde{\nu}(t) - \tilde{\nu}(\infty)}{\tilde{\nu}(0) - \tilde{\nu}(\infty)} \qquad \text{eq 1}$$

$$S_\sigma(t) = \sqrt{\frac{\tilde{\sigma}^2(t) - \tilde{\sigma}^2(\infty)}{\tilde{\sigma}^2(0) - \tilde{\sigma}^2(\infty)}} \qquad \text{eq 2}$$

In eq 1, $S_\nu(t)$ measures how the average transition-energy of the solute–solvent system relaxes with time,[1, 17-19] which can be interpreted rather intuitively. Meanwhile, in eq 2, time evolution of the spectral bandwidth is assessed with $S_\sigma(t)$.[17] If we assume that the dynamics, of both ground and excited states, follows a Gaussian-Markovian process, as well as the harmonic adiabatic potential curves hold for both electronic states, $S_\nu(t)$ and $S_\sigma(t)$ should agree with each other.[16] In experiments, on the other hand, Nishiyama and Okada found that $S_\sigma(t)$ in organic solvents at room temperature relaxes an order of magnitude slower than $S_\nu(t)$, whereas these functions relax in a somewhat similar manner in alcoholic solvents at low temperature.[7, 9] Detailed mechanisms that account for such differences in $S_\nu(t)$ and $S_\sigma(t)$ behaviors, however, have been kept unclear.

In the present study, we revisit solvation dynamics detected with transient hole-burning spectroscopy. Equilibrium molecular dynamics (MD) simulation is employed to calculate transient hole-burning spectra, where the ensemble average is replaced with the time average over the duration of the simulation run. On the basis of the MD data-sets, the transient hole-burning spectra and correlation functions that characterize the relaxation processes are derived. The results from MD simulation are compared to our spectroscopy performed previously,[7, 9] or they are analyzed with a further model using diffusion equation. The relation between solvation dynamics and harmonic, or anharmonic nature, of the reaction potential is focused.

2. System Description and MD Simulation Details

2–1. Choice of the solute–solvent systems

Acetamide and tetrahydrofuran (THF) are chosen as organic solutes. THF, acetonitrile, and methanol are used as typical organic solvents. These choices are made keeping realistic solute–solvent systems used in spectroscopy in mind. Notably, solvents are selected from protic and aprotic groups having low viscosity at room temperature. We calculate the transient hole-burning spectra using equilibrium MD simulation in organic solute X–solvent Y systems, which are hereafter denoted as "X/Y". In this study, the MD simulation is performed for the four systems: acetamide/THF, acetamide/acetonitrile, acetamide/methanol, and THF/THF.

2–2. Method to calculate transient hole-burning spectra by equilibrium MD simulation

In a solute–solvent system, we define classical Hamiltonian of the solute in the ground and excited states, as $\hat{H}_{\mathrm{g}}(\Gamma)$ and $\hat{H}_{\mathrm{g}}(\Gamma) + \Delta\hat{H}(\Gamma)$, respectively, where Γ stands for the canonical coordinate in the phase space. All the nuclear degrees of freedom are included in Γ, so that the quantum nature

of intramolecular vibrational modes is neglected. The ground-state Hamiltonian, $\hat{H}_{\mathrm{g}}(\Gamma)$, describes solute–solvent and solvent–solvent intermolecular interactions together with the intramolecular vibrational modes. The coupling, $\Delta\hat{H}(\Gamma)$, represents the variations in the solute–solvent interaction and the intramolecular geometrical change on the electronic excitation of the solute. We then express the spectrum of the excitation pulse as $w(\Delta E)$, with the energy difference of the excited and ground states, ΔE. The time-dependent depletion of the ground-state distribution, or the transient hole-burning spectrum at just after the photo-excitation, is proportional to $w\left[\Delta\hat{H}(\Gamma)\right]\rho_{\mathrm{g,eq}}(\Gamma)$, where $\rho_{\mathrm{g,eq}}(\Gamma)$ is the distribution of the ground equilibrium state. The distribution develops with time following the time-evolution operator $\hat{L}_g$ that corresponds to $\hat{H}_g(\Gamma)$. The distribution at t is thus given by $\exp\left(i\hat{L}_g t\right)w\left[\Delta\hat{H}(\Gamma)\right]\rho_{\mathrm{g,eq}}(\Gamma)$. The transient hole-burning spectrum, $I(\Delta E, t)$, is therefore provided as:

$$I(\Delta E, t) \propto \int d\Gamma \delta\left(\Delta E - \Delta\hat{H}(\Gamma)\right)\exp\left(i\hat{L}_g t\right)w\left[\Delta\hat{H}(\Gamma)\right]\rho_{\mathrm{g,eq}}(\Gamma)$$

$$= \langle\delta\left(\Delta E - \Delta\hat{H}(\Gamma;t)\right)w\left[\Delta\hat{H}(\Gamma;0)\right]\rangle_{\mathrm{g}} \qquad \text{eq 3}$$

where a statistical average concerning the ground state $\langle\cdot\rangle_{\mathrm{g}}$ is employed. We stress here that the non-equilibrium response after the photo-excitation is replaced with the equilibrium time-correlation function under $\hat{H}_g(\Gamma)$ in eq 3. We can therefore estimate $I(\Delta E, t)$ through equilibrium MD simulation regarding the ground-state solute, where time-correlation functions presented in eqs 1 and 2 are calculated. In the non-equilibrium response described in the first line of eq 3, the initial distribution deviates from the equilibrium one, whereas the time propagation follows the ground-state Hamiltonian. Its transformation into the equilibrium time correlation function in eq. 3 can thus be regarded as the reconstruction of the non-equilibrium distribution from the

equilibrium one by means of reweighting, as is performed in generalized ensemble simulations. The spectrum of the excitation pulse, $w(\Delta E)$, plays a role of the weighting factor here. Eq. 3 does not involve any approximation, just as the generalized ensemble simulations. In our algorithm, what we have to do is just to record the time profile of $\Delta\hat{H}(\Gamma)$ during the simulation run and calculate the time-correlation functions afterward. In one sense, every time in the simulation run is regarded as the excitation time, $t = 0$, and the ensemble average is replaced with the time average over the simulation run. Upon the photo-excitation, $w(\Delta E)$ is set to have a Gaussian structure whose standard deviation is given as σ_{ex}.

2–3. Computational details of MD simulation

Details of MD simulation we have performed are as follows. The simulation is executed under the isothermal–isobaric (NPT) ensemble with 298.15 K and 1.0 bar by a GROMACS 2016.5 package.[20] We employ Nosé–Hoover temperature coupling and Parrinello–Rahman pressure coupling. 999 solvent molecules and a solute molecule are included in a cubic simulation-box with a periodic boundary condition. The equation of motion is integrated using a velocity Verlet algorithm with the time step of 1 fs. We carry out an equilibration MD simulation run of 1 ns for each system, which is followed by 100 ns simulation for the data production. $\Delta\hat{H}(\Gamma)$ is recorded by every 10 fs, the time sequence of which is used to calculate transient hole-burning spectra.

The force field parameters for the solvents THF, acetonitrile, and methanol are taken from the OPLS–AA parameter set.[21] Concerned with the solutes of acetamide and THF, the OPLS–AA and GAFF[22-23] parameter sets are respectively employed except partial charges. The partial charges

of the solutes, corresponding to their isolated state, are determined by the restrained electrostatic potential (RESP) method using the density functional theory (DFT). For DFT calculations, we employ the functional of Becke–Lee–Yang–Parr with a long range correlation (LC-BLYP)[24] and a 6-31++G(d, p) basis set using a GAMESS program package.[25] The partial charges of the excited state are determined by the time-dependent density functional theory (TD-DFT) employing the same condition with that of the ground state. All the quantum-chemical calculations are performed in gas phase. The partial charges of solutes determined accordingly are summarized in Table S1 in the Supporting Information. We also comment here that the calculation procedures of the solute partial-charges described above is still reasonable, even though we use the solutes in the isolated state, not in a solution phase. The present study intends to discuss different relaxation dynamics found in the spectral peak shift and bandwidth, which can be derived adequately within our calculation. Besides, on the solute photo-excitation, the partial charges of the solute experience rearrangement, while the solute geometry is kept unchanged. Applicability of such a model is detailed in section S2–1.

3. Results and Discussion

3–1. Absorption spectra

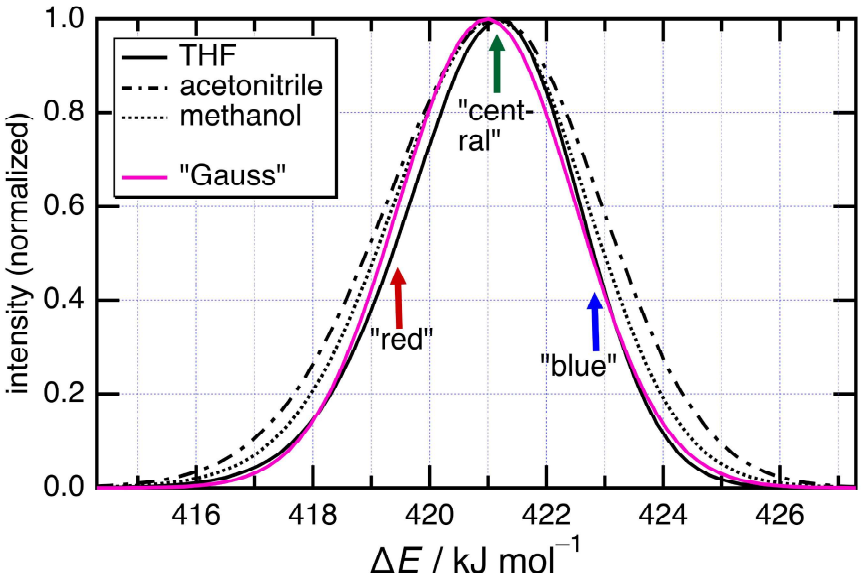

Figure 1. Normalized absorption spectra of acetamide. Solvents used are indicated in the figure. A Gaussian curve, whose first and second cumulants are identical to those in THF, is overlaid for comparison. The arrows represent the excitation positions E_{ex} shown in Figure 3. See also Figure S2a$_2$ in which the identical data-set is plotted on a logarithmic scale.

Figure 1 represents the absorption spectra of acetamide calculated for the organic solvents noted in the figure. In Figure 1, the abscissa ΔE is defined comprising the vertical transition energy between the ground and excited states, and the intramolecular Coulombic interaction-energy, of the solute (see section S2–1). All the spectra seem to have a Gaussian character, with some

asymmetric structures in both their red and blue spectral ends. The spectra reach their maxima at approximately 421 kJ mol^{-1} (or 284 nm, converted to an optical scale), irrespective of solvent. This energy is ascribed to an $n \rightarrow \pi^*$ transition of acetamide. The other properties drawn from the absorption spectra, including the dispersion (σ_{abs}^2) and full width at half maximum (fwhm), are listed in Table 1.

Table 1. σ_{abs}^2 and fwhm for the absorption spectra of acetamide in solvents

Solvent	σ_{abs}^2 / (kJ mol^{-1})^2	fwhm$^{(1)}$ / kJ mol^{-1}
THF	2.3	3.6
acetonitrile	3.5	4.4
methanol	2.9	4.0

$^{(1)}$fwhm = $2\sqrt{2\ln 2}\sigma_{abs}$

3–2. Time-correlation functions

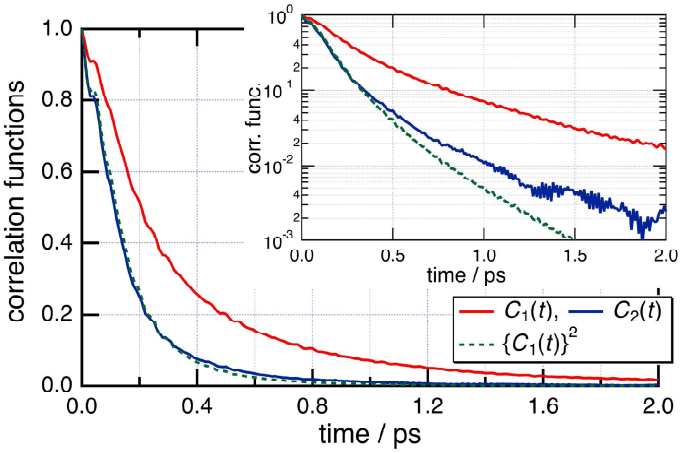

Figure 2. Time-correlation functions $C_1(t)$ (solid red line), $C_2(t)$ (solid blue line), and $\{C_1(t)\}^2$ (broken green line) calculated for acetamide/THF. The identical data-sets are plotted in the inset on a logarithmic scale. See section S3 for a detailed analysis which includes the correlation functions for the other systems and curve fitting results.

We then calculate the solvation time-correlation functions, $C_1(t)$, $C_2(t)$, and $\{C_1(t)\}^2$, where subscripts 1 and 2 indicate the first and second cumulants, respectively. Calculation methods of these functions are as follows. We compute $E(t) = \epsilon(t) - \overline{\epsilon(t)}$ where $\epsilon(t)$ is the Franck–Condon energy difference between the ground and excited states, and the overbar expresses the average. The time-correlation functions we seek are given as:

$$C_1(t) = \langle E(0)E(t)\rangle \qquad \text{eq 4}$$

$$C_2(t) = \langle \delta\sigma^2(0)\delta\sigma^2(t)\rangle \qquad \text{eq 5}$$

where $\sigma^2(t) = \{E(t)\}^2 - \langle E(t)\rangle^2$, and $\langle\cdot\rangle$ means an ensemble average. Finally, $\delta\sigma^2(t) = \sigma^2(t) - \overline{\sigma^2(t)}$ is derived.

Figures 2 and S3 represent the time-correlation functions. Note that assuming linear response, $C_1(t)$ and $C_2(t)$ correspond to $S_\nu(t)$ and $\{S_\sigma(t)\}^2$, respectively. In this context, the dynamic properties $\Delta E(t)$ and $\sqrt{\sigma^2(t)}$, or $\{\Delta E(t)\}^2$ and $\sigma^2(t)$, respectively, serve as direct comparisons. We also comment that if a Gaussian process is applicable to solvation dynamics, $\{C_1(t)\}^2 \propto C_2(t)$ should hold.[17] A prominent behavior found here is that $\{C_1(t)\}^2$ and $C_2(t)$ relax in quite different manners at $t \geq 0.3$ ps, irrespective of initial dynamics (see Figure 2 inset). Such a discrepancy, detected in all the systems, implies that non-Gaussian processes are dominant in solvation, at least in the slow region ($t \geq 0.3$ ps). Some of the time-correlation functions are fit with a biexponential function to compare relaxation times, which are provided in section S3.

3–3. Transient hole-burning spectra and related dynamics

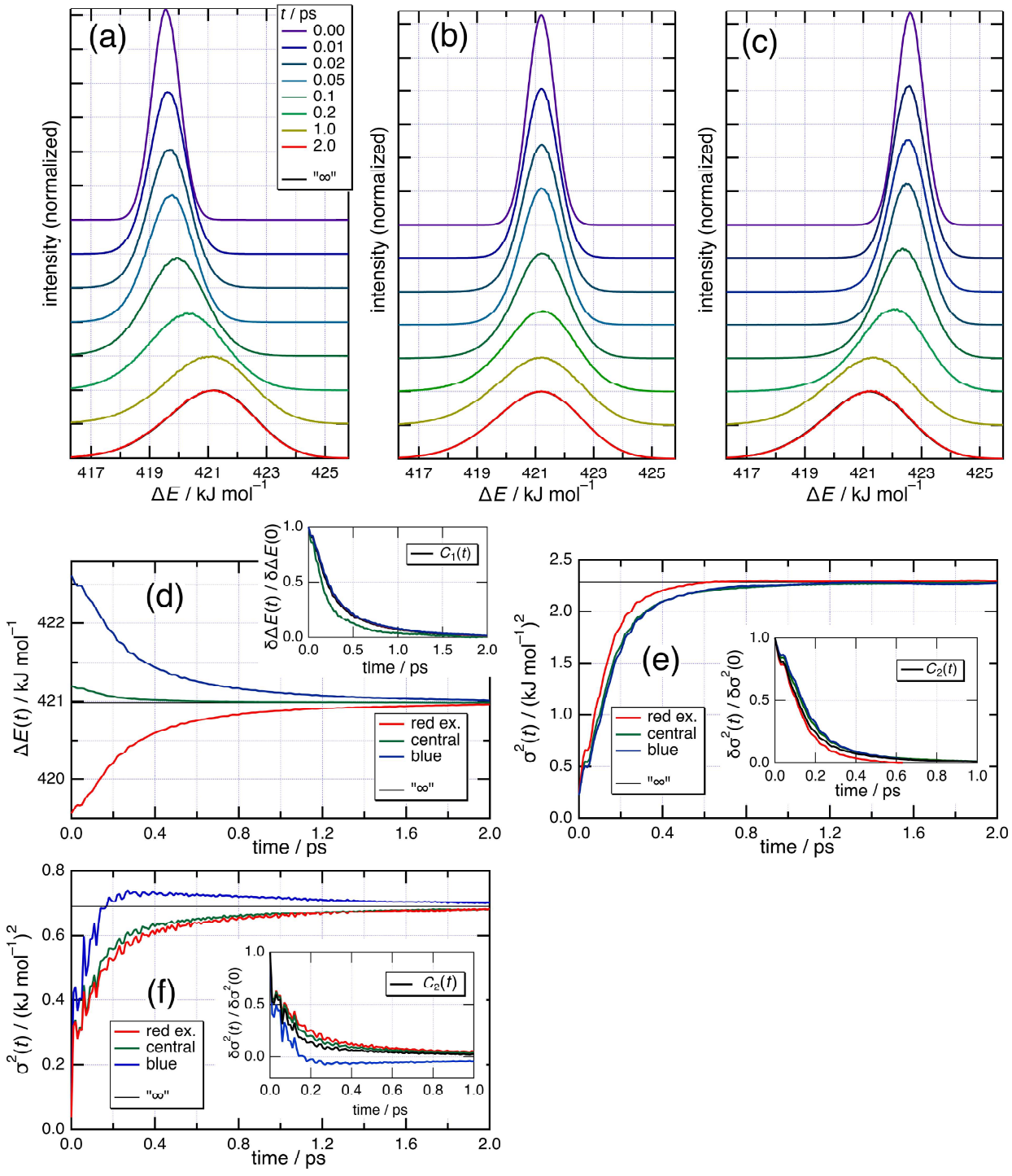

Figure 3. E_{ex} dependences of transient hole-burning spectra and related dynamics. Panels a–e are calculated for acetamide/THF, whereas panel f is for THF/THF. Panels a–c show the transient

hole-burning spectra using σ_{ex} = 0.50 kJ mol^{-1}, associated with (a) red, (b) central, and (c) blue excitation, respectively. Calculation parameters are listed in Table S3. The absorption spectrum, corresponding to the "$t = \infty$" spectrum, is shown as a black line, which almost overlaps the t = 2.0 ps spectra (red line). Panels d and e exhibit E_{ex} dependences of $\Delta E(t)$ and $\sigma^2(t)$. The $\delta\Delta E(t)/\delta\Delta E(0)$ and $\delta\sigma^2(t)/\delta\sigma^2(0)$ curves are also shown in the insets, in which their corresponding $C_1(t)$ or $C_2(t)$ curves are overlaid. Panel f displays $\sigma^2(t)$ and $\delta\sigma^2(t)/\delta\sigma^2(0)$ (inset). The thin black lines drawn horizontally in panels d–f, tagged as "∞", are the $E(t = \infty)$ or $\sigma^2(t = \infty)$ value. E_{ex} positions are provided in the panels d–f. See also Figures S4a–S4d for the data-sets for all the systems studied here.

Figures 3a–3e depict the transient hole-burning spectra and related dynamics of acetamide/THF and their dependence on E_{ex}. The spectra of the other systems can be seen in Figures S4b–S4d. The values of E_{ex} are chosen as the red, central, and blue positions of the absorption spectrum, which are depicted as arrows in Figure 1. The transient hole-burning spectra clearly depend on E_{ex}; the t = 0 spectra have their peaks in the vicinity of E_{ex}. The peak shifts are remarkable when excitation is applied on the red or blue side (Figures 3a and 3c, respectively), and subtle when central excitation is applied (Figure 3b). The spectra broaden with time irrespective of E_{ex}, finally matching those of the equilibrium absorption spectrum shown in the black line (Figure 3e). Regardless of E_{ex}, the essential part of relaxation, in terms of the spectral functions, ceases within 2 ps. The standard deviation of the excitation energy is set to σ_{ex} = 0.50 kJ mol^{-1} for the spectra in Figures 3a–3c, and to σ_{ex} = 0.05 kJ mol^{-1} for those in Figures S4a'$_1$–S4a'$_3$. The essential part of the hole and related dynamics is shown to be independent of the choice of σ_{ex}. See also section S5–1 for the choice of σ_{ex}.

Various dynamics can be derived from transient hole-burning spectra drawn in Figures 3a–3c. The first moment $\Delta E(t)$ and its quantity scaled to 0–1, $\delta\Delta E(t)/\delta\Delta E(0)$, are respectively given as:

$$\Delta E(t) = \int I(\Delta E, t)\Delta E \, \mathrm{d}\Delta E \qquad \text{eq 6}$$

$$\frac{\delta\Delta E(t)}{\delta\Delta E(0)} = \frac{\Delta E(t) - \Delta E(\infty)}{\Delta E(0) - \Delta E(\infty)} \qquad \text{eq 7}$$

where $I(\Delta E, t)$ stands for the spectral function of the transient hole-burning, with a normalized format in this context, which is obtained from eq 3. Notably, $\delta\Delta E(t)/\delta\Delta E(0)$ is compared to $S_1(t)$

(see eq 1), which is detected with spectroscopy. $\sigma^2(t)$ is calculated as dispersion of the transient hole-burning spectra, where the ensemble average is taken for calculation. The quantity $\delta\sigma^2(t)/\delta\sigma^2(0)$, which is normalized to 0–1, is obtained as:

$$\frac{\delta\sigma^2(t)}{\delta\sigma^2(0)} = \frac{\sigma^2(t) - \sigma^2(\infty)}{\sigma^2(0) - \sigma^2(\infty)} \qquad \text{eq 8}$$

We state that $\delta\sigma^2(t)/\delta\sigma^2(0)$ is compared with $\{S_\sigma(t)\}^2$, in eq 2, which is also detected with spectroscopy.

Figures 3d and 3e indicate $\Delta E(t)$ and $\sigma^2(t)$ for acetamide/THF, respectively, along with their normalized quantities shown in the insets. In Figure 3d, the $\Delta E(t = 0)$ values begin with their E_{ex} positions. With time, $\Delta E(t)$ curves with both red- and blue-side excitations approach toward $\Delta E(t = \infty)$, which corresponds to the energy at the spectral maximum of absorption. The $\delta\Delta E(t)/\delta\Delta E(0)$ curves converge to zero by 1.5–2.0 ps after the excitation. The curves with the red and blue excitations overlap with each other (Figure 3d inset), which tells us the relaxation dynamics are almost independent of the E_{ex} positions.

Using the central excitation drawn in the green curve in the Figure 3d inset, $\delta\Delta E(t)/\delta\Delta E(0)$ curve appears to relax in a slightly different manner than those with the other excitation conditions. The reason for this difference is ascribed to statistical fluctuation, which roots in the least amount of energy to be relaxed. The central-excitation curve relaxes from $\Delta E(t = 0) = 421.20$ kJ mol^{-1} to $\Delta E(t = \infty) = 420.99$ kJ mol^{-1}. Therefore, the relaxing energy is only ~0.2 kJ mol^{-1} in this process, in its absolute amount. Notably, the relaxing energy is much more for the red and blue excitations

(~1.5 kJ mol^{-1}). Such general dynamic behaviors in $\Delta E(t)$, or in $\delta\Delta E(t)/\delta\Delta E(0)$ as derived, have been observed in other systems (see Figures S4a–4d).

We turn our attention to specific behavior of $\sigma^2(t)$ curves. Figure 3e represents the $\sigma^2(t)$ curves for acetamide/THF depending on E_{ex}, and $\delta\sigma^2(t)/\delta\sigma^2(0)$ are shown in the inset. The $\delta\sigma^2(t)/\delta\sigma^2(0)$ curves are rather independent of E_{ex}, and their three curves are almost similar to the $C_2(t)$ decay, apart from some minor differences. Similar results have been detected also for acetamide/acetonitrile and acetamide/methanol (see Figures S4b and S4c, respectively). By contrary, the $\sigma^2(t)$ curve for THF/THF with the blue excitation (Figure 3f) exhibits a peculiar behavior; once the curve reaches its maximum at t = 0.3 ps, it is followed by a slow relaxation as its value is reduced to reach equilibrium at ~2.0 ps. This "overshot" behavior was also reported in relation to time-resolved fluorescence measurements using an organic probe, coumarin 153, with the blue excitiation.[26] Note that the blue excitation curve for acetamide/THF relaxes in a similar manner to the other curves, as seen in Figure 3e.

3–4. Dynamics obtained from the diffusion model

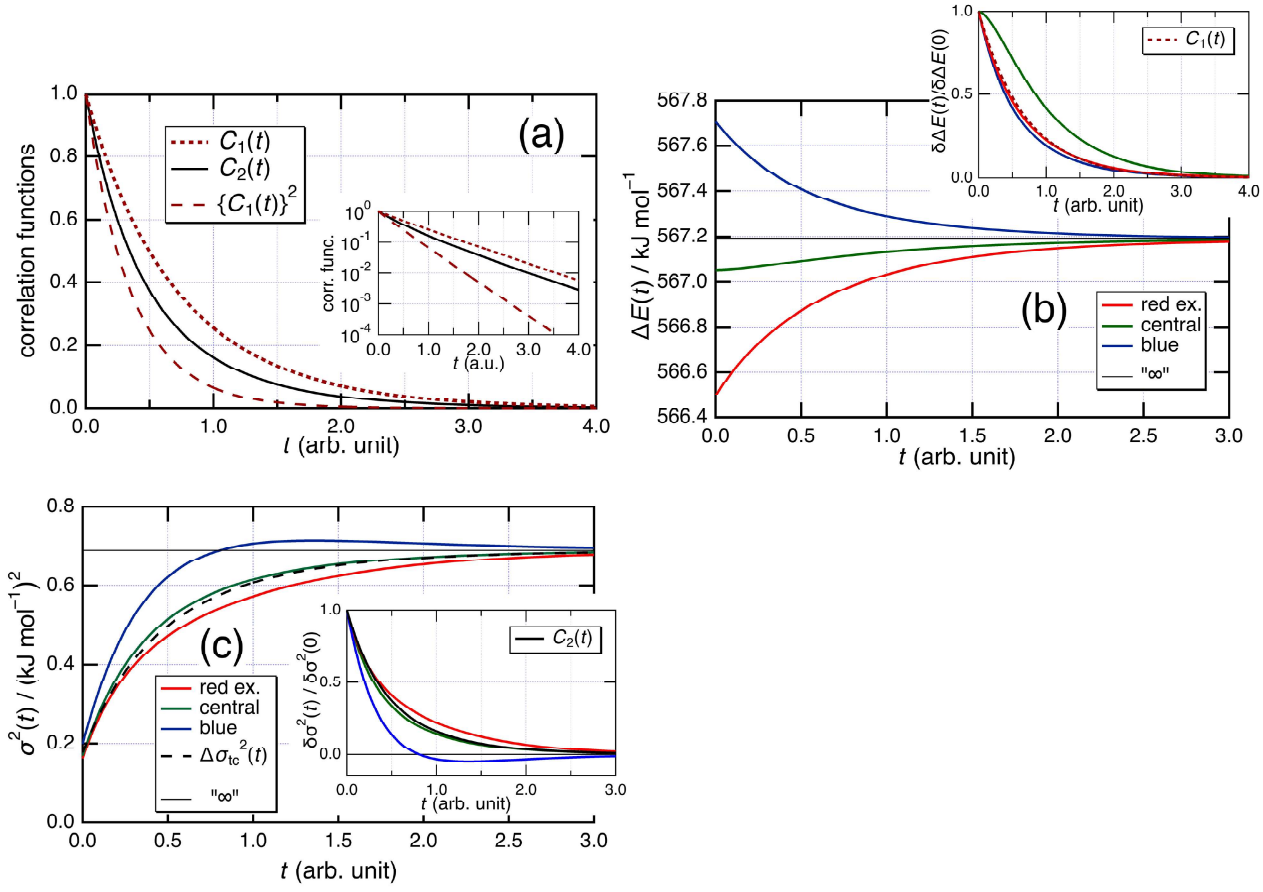

Figure 4. Time-correlation functions and related dynamics obtained from the diffusion model for THF/THF, where all the relaxations are supposed to follow the diffusive equation. The abscissa, t, is in an arbitrary scale, which is defined by D in eq 9. Panel a shows $C_1(t)$, $C_2(t)$, and $\{C_1(t)\}^2$, normalized with their $t = 0$ values, and the identical data-sets are plotted in a logarithmic scale in the inset. E_{ex} dependences for panels (b) $\Delta E(t)$ and (c) $\sigma^2(t)$ with $\Delta\sigma_{tc}^2(t)$, are also shown, along with their normalized quantities in the insets. Their equilibrium values obtained at $t = \infty$ are also provided. The ordinate of panel b is calculated with eq S3. The time-correlation functions are analyzed with biexponential curves, whose results are given in section S6.

The MD simulation presented above indicates that $\sigma^2(t)$ relaxes much more slowly than $\Delta E(t)$, and the relaxation dynamics clearly depends on E_{ex}. Such results suggest that a non-Gaussian process is responsible for solvation. We therefore employ the diffusion equation to elucidate whether the nonlinearity could be the central reason for the non-Gaussian character:

$$\frac{\partial}{\partial t}\rho(x,t) = D\frac{\partial}{\partial x}\left[\rho(x,t)\frac{\partial}{\partial x}\ln\frac{\rho(x,t)}{\rho(x,t=\infty)}\right] \qquad \text{eq 9}$$

where ρ stands for the ground-state distribution that relaxes along the potential, and $\rho(x, t = \infty) \propto I(x = \Delta E, t = 0)$ is obtained from the MD simulation. D is the diffusion constant. Eq 9 is the diffusion equation under the external potential, where $-k_B T ln\rho(x, t = \infty)$ plays the role of the free-energy profile along the solvation coordinate. Some of the absorption spectra, $I(\Delta E, t=0)$, are plotted in a logarithmic scale in section S2–2, which indicates the anharmonicity of the free-energy profile.

Figures 4a–4c display time-correlation functions, $\Delta E(t)$, $\sigma^2(t)$, and their normalized quantities, calculated using eq 9 for THF/THF. The t axis is provided in an arbitrary scale, which is coupled with D. The functions are analyzed with a biexponential function, whose results are presented in section S6. In the main panel of Figure 4a, different behaviors are found in the $C_1(t)$ and $C_2(t)$ curves in their early stages ($t \leq 1$). However, their long-tail components, or the decay-line slopes, are quite similar (see inset). Moreover, in Figure 4c, the $\sigma^2(t)$ curve associated with the blue excitation at first becomes broader than its equilibrium value, $\sigma^2(t = \infty)$, and then shrinks. Such overshot behavior has also been found in our MD result for the same system (Figure 3f). In Figure 4c, we also present $\Delta\sigma_{tc}^2(t)$, in which the time-dependent spectral bandwidth is

reconstructed using $C_2(t)$ obtained from the diffusion model. We are aware that $\Delta\sigma_{tc}^2(t)$ corresponds roughly to the $\sigma^2(t)$ curve with central excitation.

3–5. Non-Gaussian aspects of hole dynamics

An essential conclusion drawn from the present MD simulation is that the non-Gaussian property of the hole dynamics is characterized by anharmonicity of the free energy profile of the absorption spectra. Such a property leads to the difference in behavior between $\{C_1(t)\}^2$ and $C_2(t)$. Given an anharmonic free energy potential, we *shall* encounter different $\{C_1(t)\}^2$ and $C_2(t)$ behaviors as a universal phenomenon.[16] At low temperature, where relaxation is related to a small vibration around the local minimum of the free energy potential, $\{C_1(t)\}^2$ and $C_2(t)$ would agree with each other. In reality, for dye molecules in alcohols at low temperature (160 K), they relax in a similar manner.[9, 27] However, at room temperature, much more thermal fluctuation is possible in solvent; which would enhance the nonlinear characteristics of the ground-state potential.

Another case of a harmonic potential may be found in systems where the central limit theorem holds. Systems comprising a large number of relaxing agents or solvents would behave in a Gaussian manner, even though the individual modes behave in an anharmonic manner. Dye molecules used typically in realistic spectroscopy are much larger than the solutes employed in this study. Therefore, the anharmonicity should appear more clearly in the present systems. Even in realistic solutes, systems where specific functional groups are responsible for static or dynamic spectral changes are often found. For instance, solvation probes where a carbonyl moiety is introduced to an oxazine ring are sometimes used. A dominant dipole-moment change occurs around the C=O moiety upon photo-excitation,[26, 28] which brings about significant solvent-rearrangements in close proximity to the moiety.[28] Dynamics driven by anharmonicity is also

essentially attributed to that region.[26] On the other hand, a system in which many solvents take part in the relaxation may demonstrate a Gaussian process due to the central limit theorem.

The anharmonicity detected in solvation dynamics presently has an origin in solute–solvent interactions, essentially. If a solute with a huge geometry is used, the response from such a system would not be "averaged" by the central limit theorem. Anharmonicity with a large magnitude would thus be detected. Otherwise, a system with strong solute–solvent interactions may provide more explicit anharmonicity in the system response. An example for such systems can be found in those with hydrogen bonding solvents. Actually, a solvent group with the hydrogen bond is reported to give departures regarding spectral shifts than the others.[26]

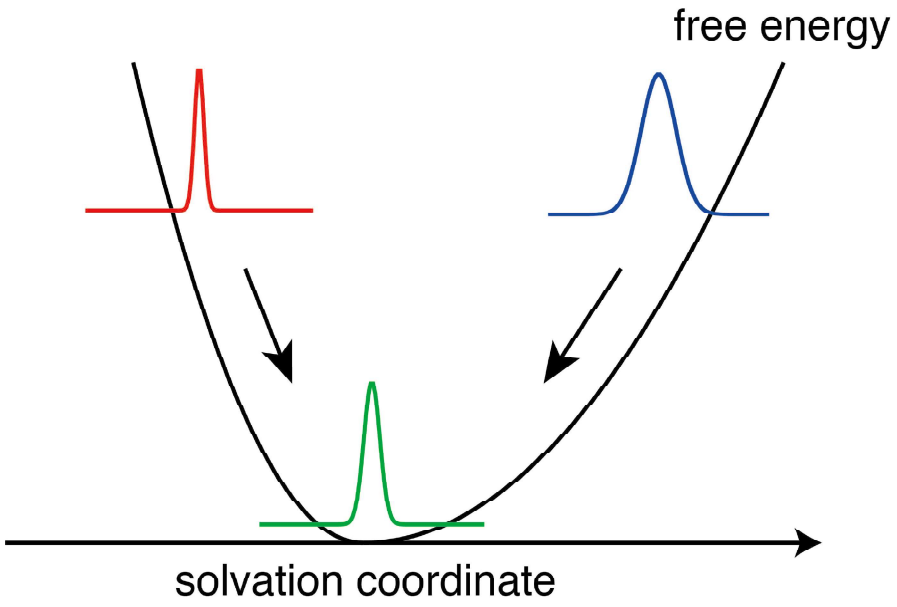

Chart 2. A diagram showing the dynamic evolution of transient hole-burning spectra, associated with anharmonicity of the ground-state potential.

Chart 2 shows a schematic of the hole relaxation described in the present study. Due to anharmonicity of the free energy potential, the relaxation dynamics clearly depends on E_{ex}. With the red excitation, where the curvature of the potential is rather steep, the hole travels toward the bottom of the potential and $\sigma^2(t)$ increases with time. Notably, the curvature at which the hole "feels" during the travel decreases with time evolution. Eventually, $\delta\Delta E(t)/\delta\Delta E(0)$ and $\delta\sigma^2(t)/\delta\sigma^2(0)$ relax in a similar manner.

On the other hand, with the blue excitation, $\sigma^2(t)$ increases in the early stage of relaxation and then decreases toward equilibrium. The curvature where the hole stays is small at first, and then increases as the hole travels to the bottom of the potential. The overshot relaxation observed

for THF/THF with the blue excitation, using both MD simulation and the diffusion equation, can also be explained with this scheme.

4. Conclusions

We studied the origins of the different relaxation dynamics experimentally observed in the spectral peak and bandwidth, where the latter relaxes approximately an order of magnitude slower. In this report, we presented a new methodology to calculate transient hole-burning spectra based on equilibrium MD simulation. In the simulation, an ensemble average is replaced with the time average over the duration of the simulation run. The MD results obtained here sufficiently reproduced the different dynamics which has been reported experimentally. The difference regarding dynamics of the bandwidth and peak shift, detected by both experiments and MD simulation, has been ascribed to anharmonicity of the free energy potential. To our knowledge, this can be the very first report which develops the method where equilibrium MD simulation is used to derive the transient hole-burning spectra. As a future perspective, development of MD simulation makes calculations of more realistic solute–solvent systems possible, and we will derive solvation dynamics in a more detailed sense. Such systems with larger solutes should exhibit less non-Gaussian behaviors in their dynamic behaviors. In this context, further studies using experimental and simulation methods are indeed desirable, to elucidate molecular origins of relaxation dynamics which characterizes the spectral peak and bandwidth.

ASSOCIATED CONTENT

Supporting Information.

The Supporting Information is available free of charge on the ACS Publications website. Partial charges of solutes; Details of absorption spectra; Time-correlation functions; Excitation conditions for transient hole-burning spectra; Details of transient hole-burning spectra and related dynamics; Fitting curves for $C_1(t)$, $C_2(t)$, and $\{C_1(t)\}^2$ obtained from the diffusion model for THF/THF (PDF)

AUTHOR INFORMATION

Corresponding Authors

Tsuyoshi Yamaguchi

E-mail: yamaguchi.tsuyoshi@material.nagoya-u.ac.jp

Phone: +81–52–789–3592

Katsura Nishiyama

E-mail: knis@meijo-u.ac.jp

Phone: +81–52–832–1151

Notes

The authors declare no competing financial interests.

ACKNOWLEDGMENT

We thank financial support from JSPS KAKENHI (Grant Numbers 16H00842 and 16K05519 to NY, 16K05750 to KN). NY acknowledges the Toyota Riken Scholar from Toyota Physical and Chemical Research Institute, and KN Hibi Science Foundation.

REFERENCES

1. Bagchi, B.; Oxtoby, D. W.; Fleming, G. R., Theory of the Time Development of the Stokes Shift in Polar Media. *Chem. Phys.* **1984,** *86*, 257–267.
2. Rosenthal, S. J.; Xie, X.; Du, M.; Fleming, G. R., Femtosecond Solvation Dynamics in Acetonitrile: Observation of the Inertial Contribution to the Solvent Response. *J. Chem. Phys.* **1991,** *95*, 4715–4718.
3. Maroncelli, M., The Dynamics of Solvation in Polar Liquids. *J. Mol. Liq.* **1993,** *57*, 1–37.
4. Cho, M.; Yu, J.-Y.; Joo, T.; Nagasawa, Y.; Passino, S. A.; Fleming, G. R., The Integrated Photon Echo and Solvation Dynamics. *J. Phys. Chem.* **1996,** *100*, 11944–11953.
5. Kinoshita, S.; Itoh, H.; Murakami, H.; Miyasaka, H.; Okada, T.; Mataga, N., Solvent Relaxation Effect on Transient Hole-Burning Spectra of Organic Dyes. *Chem. Phys. Lett.* **1990,** *116*, 123–127.
6. Kang, T. J.; Yu, J.; Berg, M., Rapid Solvation of a Nonpolar Solute Measured by Ultrafast Transient Holeburning. *Chem. Phys. Lett.* **1990,** *174*, 476–480.
7. Nishiyama, K.; Asano, Y.; Hashimoto, N.; Okada, T., Solvation Dynamics of Dye Molecules in Polar Solvents Studied by Time Resolved Hole Burning Spectroscopy. *J. Mol. Liq.* **1995,** *65/66*, 41–48.
8. Ma, J.; Bout, D. V.; Berg, M., Transient Hole Burning of *s*-Tetrazine in Propylene Carbonate: A Comparison of Mechanical and Dielectric Theories of Solvation. *J. Chem. Phys.* **1995,** *103*, 9146–9160.
9. Nishiyama, K.; Okada, T., Relaxation of Inhomogeneous Spectral Band Width of Dye Molecules in Polar Solvents Studied by Time-Resolved Hole and Fluorescence Spectroscopy. *J. Phys. Chem. A* **1997,** *101*, 5729–5735.
10. Nishiyama, K.; Okada, T., Relaxation Dynamics of Inhomogeneous Spectral Width in Binary Solvents Studied by Transient Hole-Burning Spectroscopy. *J. Phys. Chem. A* **1998,** *102*, 9729–9733.
11. Jumper, C. C.; Arpin, P. C.; Turner, D. B.; McClure, S. D.; Rafiq, S.; Dean, J. C.; Cina, J. A.; Kovac, P. A.; Mirkovic, T.; Scholes, G. D., Broad-Band Pump-Probe Spectroscopy

Quantifies Ultrafast Solvation Dynamics of Proteins and Molecules. *J. Phys. Chem. Lett.* **2016,** *7*, 4722–4731.

12. Elola, M. D.; Rodriguez, J.; Laria, D., Liquid Methanol Confined within Functionalized Silica Nanopores. 2. Solvation Dynamics of Coumarin 153. *J. Phys. Chem. B* **2011,** *115*, 12859–12867.
13. Haldrup, K.; Gawelda, W.; Abela, R.; Alonso-Mori, R.; Bergmann, U.; Bordage, A.; Cammarata, M.; Canton, S. E.; Dohn, A. O.; van Driel, T. B. et al., Observing Solvation Dynamics with Simultaneous Femtosecond X-Ray Emission Spectroscopy and X-Ray Scattering. *J. Phys. Chem. B* **2016,** *120*, 1158–1168.
14. Najafi, M.; Herascu, N.; Seibert, M.; Picorel, R.; Jankowiak, R.; Zazubovich, V., Spectral Hole Burning, Recovery, and Thermocycling in Chlorophyll − Protein Complexes: Distributions of Barriers on the Protein Energy Landscape. *J. Phys. Chem. B* **2012,** *116*, 11780−11790.
15. Lvovsky, A. I.; Sanders, B. C.; Titte, W., Optical Quantum Memory. *Nat. Photon.* **2009,** *3*, 706–714.
16. Kinoshita, S., Theory of Transient Hole-Burning Spectrum for Molecules in Solution. *J. Chem. Phys.* **1989,** *91*, 5175–5184.
17. Kinoshita, S.; Nishi, N.; Kushida, T., Stochastic Behavior of the Dynamic Stokes Shift in Rhodamine 6g. *Chem. Phys. Lett.* **1987,** *134*, 605–609.
18. E. W. Castner, J.; Maroncelli, M.; Fleming, G. R., Subpicosecond Resolution Studies of Solvation Dynamics in Polar Aprotic and Alcohol Solvents. *J. Chem. Phys.* **1987,** *86*, 1090–1097.
19. Kahlow, M. A.; Kang, T. J.; Barbara, P. F., Transient Solvation of Polar Dye Molecules in Polar Aprotic Solvents. *J. Chem. Phys.* **1988,** *88*, 2372–2378.
20. Berendsen, H. J. C.; Spoel, D. v. d.; Drunen, R. v., Gromacs: A Message-Passing Parallel Molecular Dynamics Implementation. *Comput. Phys. Commun.* **1995,** *91*, 43–56.
21. Jorgensen, W. L.; Maxwell, D. S.; Tirado-Rives, J., Development and Testing of the Opls All-Atom Force Field on Conformational Energetics and Properties of Organic Liquids. *J. Am. Chem. Soc.* **1998,** *118*, 11225–11236.
22. Wang, J.; M.Wolf, R.; Caldwell, J. W.; Kollman, P. A.; Case, D. A., Development and Testing of a General Amber Force Field. *J. Comput. Chem.* **2004,** *25*, 1157–1174.

23. Wang, J.; Wang, W.; Kollman, P. A.; Case, D. A., Automatic Atom Type and Bond Type Perception in Molecular Mechanical Calculations. *J. Mol. Graph. Model.* **2006,** *25*, 247–260.
24. Yanai, T.; Tew, D. P.; Handy, N. C., A New Hybrid Exchange–Correlation Functional Using the Coulomb-Attenuating Method (Cam-B3lyp). *Chem. Phys. Lett.* **2004,** *393*, 51–57.
25. Schmidt, M. W.; Baldridge, K. K.; Boatz, J. A.; Elbert, S. T.; Gordon, M. S.; Jensen, J. H.; Koseki, S.; Matsunaga, N.; Nguyen, K. A.; Su, S. et al., General Atomic and Molecular Electronic Structure System. *J. Comput. Chem.* **1993,** *14*, 1347–1363.
26. Horng, M. L.; Gardecki, J. A.; Papazyan, A.; Maroncelli, M., Subpicosecond Measurements of Polar Solvation Dynamics: Coumarin 153 Revisited. *J. Phys. Chem.* **1995,** *99*, 17311–17337.
27. Kinoshita, S.; Nishi, N., Dynamics of Fluorescence of a Dye Molecule in Solution. *J. Chem. Phys.* **1988,** *89*, 6612–6622.
28. Nishiyama, K.; Watanabe, Y.; Yoshida, N.; Hirata, F., Solvent Dependence of Stokes Shift for Organic Solute–Solvent Systems: A Comparative Study by Spectroscopy and Reference Interaction-Site Model–Self-Consistent-Field Theory. *J. Chem. Phys.* **2013,** *139*, 094503 (11 pages).

TOC GRAPHICS